Applied Surface Science 257 (2011) 5793–5798

Contents lists available at ScienceDirect

Applied Surface Science

journal homepage: www.elsevier.com/locate/apsusc

# An XPS study of Au alloyed Al–O sputtered coatings

N.M. Figueiredo [a,*], N.J.M. Carvalho [b], A. Cavaleiro [a]

[a] SEG-CEMUC–Department of Mechanical Engineering, University of Coimbra, Coimbra, Portugal
[b] Bekaert Advanced Coatings NV, Deinze, Belgium

ARTICLE INFO

*Article history:*
Received 29 July 2010
Received in revised form 7 January 2011
Accepted 21 January 2011
Available online 1 February 2011

*Keywords:*
XPS
$Al_2O_3$–Au
Au clusters
Alumina
Charging effect

ABSTRACT

The focus of this research is the X-ray photoelectron spectroscopy (XPS) analysis of thin films consisting of Au metal clusters embedded in a dielectric matrix of Al–O coatings. The coatings were deposited by co-sputtering an Al + Au target in a reactive atmosphere with Au contents up to 8 at.%. The Al–O matrix was kept amorphous even after annealing at 1000 °C. In the as-deposited films the presence of Au clusters with sizes smaller than 1–2 nm (not detected by XRD) was demonstrated by XPS. With increasing annealing temperature, Au clustering in the dielectric matrix was also confirmed by XPS, in agreement with XRD results.



## 1. Introduction

XPS is a powerful technique that can yield valuable data about elemental composition, the oxidation state of elements and in favorable cases on the dispersion of one phase over another [1]. XPS is extensively used to study metal-oxide interactions providing information about the electronic structures at the interface and enabling the understanding of charge transfer processes at metal/oxide interfaces. Moreover, this technique is also surface-sensitive and, thus, it can detect small changes in surface chemical composition, e.g., surface diffusion and interdiffusion [2].

Nanocomposite coatings consisting of Au nanoparticles inserted in a dielectric matrix have been developed in recent years for many different applications, such as surface enhanced Raman spectroscopy (SERS), chemical and biological sensors, biomedical diagnosis and treatments, photovoltaic cells, lithography and near-field imaging, nano-wave-guides, non-linear optical devices, heat assisted magnetic recording (HAMR) and optical scissors [3]. The present paper aims to use XPS as a tool to understand the distribution (qualitatively and quantitatively) of Au atoms in an aluminum oxide matrix and the possible interactions that might occur between Au and the matrix elements, before and after thermal annealing treatments.

## 2. Experimental details

The coatings were deposited by pulsed d.c. reactive magnetron sputtering from an aluminum target incrusted with different amounts of gold in a reactive atmosphere ($Ar + O_2$). Briefly, the strategy consisted of drilling two circular holes in the target, on each side of the erosion track, and inserting gold pieces of varying length and number inside the grooves. The samples were placed in the substrate holder in front of the target not surpassing the zones defined by the incrusted Au strips. The power density applied to the target was constant at 4 W cm$^{-2}$. The deposition pressure was fixed at approximately 0.5–0.6 Pa. Before deposition, an ultimate vacuum pressure better than $1 \times 10^{-3}$ Pa was reached. All the coatings were deposited on silicon (1 1 1) plates. The substrate surface was ion cleaned with an ion gun.

The thickness of the films was determined by profilometry using a Perthometer S4P model with a type T1 RFHTB50 mechanical head. The chemical composition of the coatings was determined by Cameca SX-50 electron probe microanalysis (EPMA) apparatus with wavelength-dispersive X-ray spectroscopy (WDX) operating at 10 keV and the structure of the films was analyzed by X-ray diffraction (XRD) using a Philips (PANalytical) diffractometer with Co-Kα radiation in grazing incident configuration (GIXRD), with an incident angle of 2°. XPS data were acquired by using a Physical Electronics Quantum 2000 Scanning ESCA Microprobe. This system uses monochromatized Al-Kα radiation ($h\nu$ = 1486.6 eV) as the excitation source. The analyzer with a take-off angle of 45° was operated at a constant pass energy of 23.5 eV. Depth profiling was performed using the $Ar^+$ ion gun (2.5 keV) with a sputtering rate

* Corresponding author. Tel.: +351 239 790 745; fax: +351 239 790 701.
*E-mail address:* nuno.figueiredo@dem.uc.pt (N.M. Figueiredo).

0169-4332/$ – see front matter © 2011 Elsevier B.V. All rights reserved.
doi:10.1016/j.apsusc.2011.01.104

**Table 1**
Thickness results and chemical analysis by EPMA for the Au–$Al_2O_3$ composites.

| Ref. | Thickness (μm) | Atomic % ± Standard deviation | | | Al/O |
|---|---|---|---|---|---|
| | | Au | Al | O | |
| AlO-19 | 1.0 | – | 36.2 ± 0.1 | 63.8 ± 0.1 | 0.57 |
| AlO-18 | 1.0 | 0.6 ± 0.1 | 36.2 ± 0.1 | 63.1 ± 0.2 | 0.57 |
| AlO-17 | 1.0 | 3.6 ± 0.1 | 33.1 ± 0.2 | 63.4 ± 0.1 | 0.52 |
| AlO-16 | 1.6 | 7.6 ± 0.1 | 28.7 ± 0.1 | 63.7 ± 0.2 | 0.45 |

of ∼0.1 nm/s. All the peak fittings were performed applying Shirley background correction and using the proper area relation between the doublets and a fixed spin-orbit splitting.

## 3. Basic characterization

The deposited coatings from the system Al–O–Au had gold contents from 0 up to 8 at.% (Table 1) and all the samples revealed themselves to be over-stoichiometric in oxygen with regard to $Al_2O_3$, this difference being accentuated by the increase in gold. Considering that the amount of oxygen is kept approximately constant, independent of the Au content, this result suggests that the Au is most probably substituting Al which, in such a case, would lead to an overall decrease in the Al/O ratio.

All the Al–O + Au coatings revealed to be XRD amorphous in the as-grown condition; the presence of neither gold nor Al–O matrix peaks was detected whatever the Au content was. Only for annealing temperatures equal to or above 400 °C were the first signs of Au crystallization detected for the coating with the highest gold content. The crystallinity of Au was greatly improved for higher annealing temperatures, especially at 1000 °C. The narrowing of the peaks with increasing annealing temperatures suggested different sizes of Au nanoparticles. After the application of the Scherrer equation to the integral breadth of the XRD peaks, an estimation of the size of Au nanoparticles for the sample with 7.6% at. Au at 400 °C and 1000 °C was 3 nm and 25 nm, respectively. The sample containing 3.5% at. Au only crystallized at 1000 °C and the grain size was approximately 10 nm. In any case, no signs of the crystallization of the Al–O matrix could be observed. The annealing also gave rise to blistering of the coatings, particularly at 1000 °C, where flaking off was clearly observed in several surface zones. All the results of this basic characterization are to be published soon.

## 4. XPS analysis

The charging effects frequently arising during XPS measurements were corrected by assuming that the C–C bond from the contamination layer had a binding energy (BE) of 284.7 eV in the C 1s spectrum. As the C 1s peak vanished completely after surface cleaning by ion bombardment, the internal reference for peak position correction was taken from the major contribution of the Al–O bond peak either from the O 1 s spectrum (with BE at 531.5 eV) or from the Al 2p spectrum (BE at 74.6 eV).

The Au 4f level gives two photoemission peaks, $4f_{7/2}$ and $4f_{5/2}$ with an intensity ratio of 4:3 and an energy difference, the spin-orbit splitting, of 3.65 eV [4]. The Al 2p and Si 2p levels give the $2p_{3/2}$ and $2p_{1/2}$ doublets. Their intensity ratio is 2:1 and the spin-orbit splitting of the doublets is 0.4 eV[5] and 0.6 eV [6], respectively. These values were taken into account whenever deconvolution of the peaks was performed. From now on, whenever a binding energy for the Au 4f peak is referred to it takes into account the $4f_{7/2}$ contribution. In the same way, for the Al 2p and Si 2p cases, the BE values take into account the major $2p_{3/2}$ contribution.

### 4.1. As-deposited samples

For all the as-deposited samples the O 1s spectra, achieved after the samples have been ion bombarded for surface cleaning, were deconvoluted and the main peak was fixed (Fig. 1(a)) at 531.5 eV, the characteristic value of the O–Al bond in alumina [7], serving as internal reference. As expected, the main peak in the Al 2p spectrum (Fig 1(b)) is located around 74.6 ± 0.1 eV [7], the value of the Al–O bond in that compound. In the Au doped samples, specially for the one with the highest Au content (7.6% at Au), the presence of a small shoulder in the higher energy region of both O 1s and Al 2p spectra, at ∼533.3 eV and ∼76.4 eV, respectively, was noted.

The Au 4f XPS spectrum of the sample with less gold content (0.6% at. Au) in Fig1(c) shows a peak at ∼85 eV, a value significantly higher than the BE of elemental Au, that could indicate an emission from a different, strongly electron-withdrawing chemical environment, which might be the case of isolated atoms or nano-clusters of gold surrounded by the oxide matrix [8]. This peak should not be related exclusively to Au-oxide since no new low binding energy (LBE) peak was detected in the O 1s spectrum that could indicate such an electronic transition (as compared with the sample without gold). Moreover, the oxidation of small gold Au clusters (2–13 atoms) is usually distinguished in the Au 4f XPS spectrum by a chemical shift of ∼1.5 eV [9], a value appreciably higher than the one observed in the present case. Rao et al. [10] reported, when analyzing the BE of gold deposited onto highly oriented pyrolitic graphite (HOPG) that, when going from bulk gold to gold clusters with sizes lower than 2 nm, the core-level binding energy increased to a maximum of 0.8 eV (corresponding to clusters with diameters close to 0.5 nm), this phenomenon being mainly attributed to a decrease in the core–hole screening by conduction electrons, as a result of the discretization of the conduction band [10–13]. For large clusters of diameters superior to 4 nm, the BE closely approximated the bulk metal value. Similar results were obtained by Lim et al. [14], while studying the size-selectivity in the oxidation behaviour of Au nanoparticles supported on silica surfaces, where identical positive shifts were observed in the Au 4f core level up to 0.8 eV with decreasing cluster size. In a more extensive study, Mason [11] compiled a series of observed core-level BE shifts for several metal-substrate combinations arising from the shrinking of the metallic clusters, and reported a maximum BE shift of 1.1 for the Au–$Al_2O_3$ system. However, in the current study, the Au clusters are expected to be dispersed throughout the oxide matrix, and not only on its surface, which can result in a broader range of values for the shifts in BE. In embedded clusters a possible reduction in cluster charging due to the increased contact area and the increased polarization energy can be countered by the absence of image charge screening, resulting in higher BE shifts [15]. Dalacu et al. [15] observed higher BE shifts for Au clusters embedded in $SiO_2$ than when they are simply supported in the oxide surface.

In conclusion, the peak at 85 eV in the Au 4f XPS spectrum of the sample with less gold content is hereby attributed to small gold clusters with diameters inferior than 1–2 nm (probably closer to 0.5 nm), which can be as small as isolated atoms, embedded in the Al–O matrix. The fact that this peak possesses enlarged full-width at half maximum (FWHM) when compared to bulk Au (∼2 eV compared to ∼1 eV) is also an expected result since the line-width is also believed to increase with decreasing screening; line broadenings of about 1 eV have been previously observed for small Au clusters supported in $Al_2O_3$ [11,15]. Additionally, since the BE shift increases with the decrease in cluster size, the peak broadening could indicate the presence of clusters of different sizes (broad size distribution).

At first glance, the two high binding energy (HBE) peaks occurring in the Al 2p and O 1s spectra could be attributed to a hydroxide compound, such as $Al(OH)_3$ [4]. However, this could only make

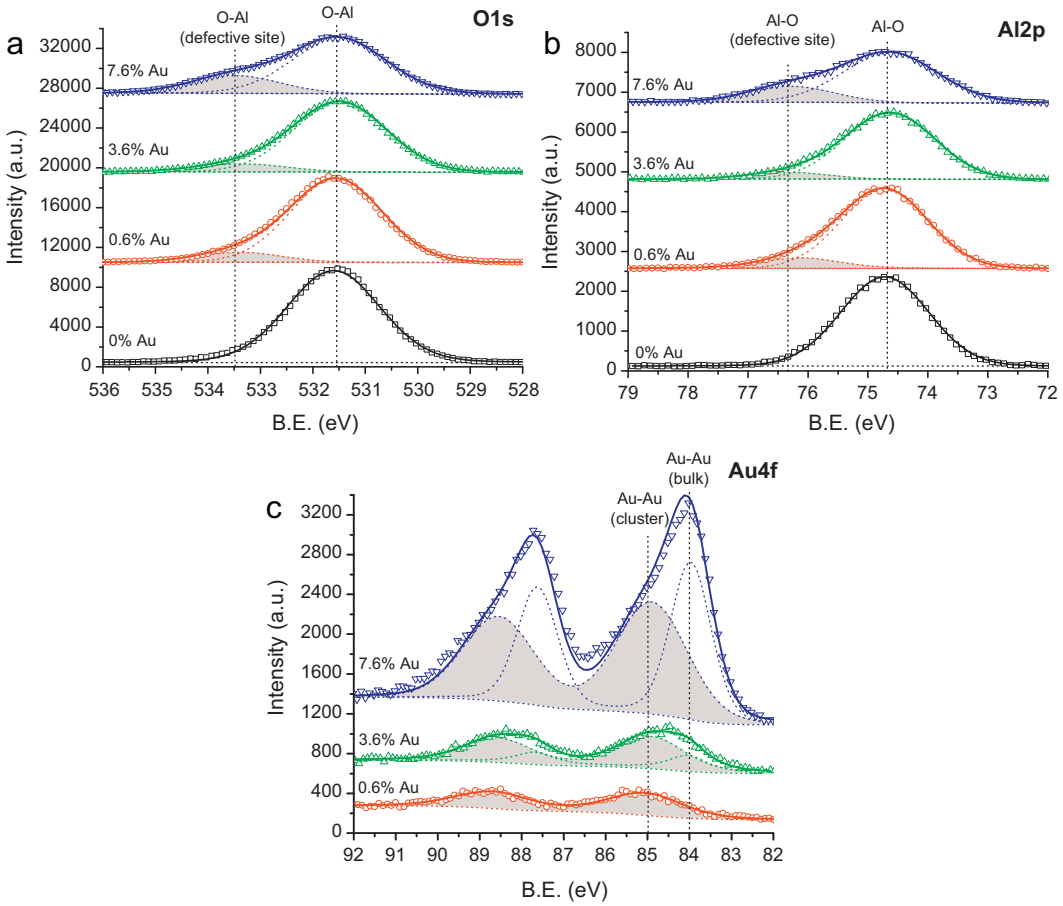


**Fig. 1.** XPS spectra and main deconvoluted contributions of (a) O 1s (b) Al 2p and (c) Au 4f peaks of as-deposited Al–O + Au coatings with increasing Au content.

sense at the surface of the samples and not throughout the depth profile after surface ion bombardment. Moreover, if such a bond existed it should be detected with similar intensities in all the samples, including the Au-free one. The HBE peaks can be explained by changes in the electron transfer between the oxide and the gold occurring during XPS analysis. The interaction of gold atoms and the alumina matrix can change significantly depending on the way the gold is arranged in relation to the matrix. Lim et al. [9] carried out an XPS study of the oxidation behavior of size-selected gold clusters (2–13 atoms) deposited on silica and graphite and observed that the chemical properties of the Au clusters drastically changed with the number of atoms and could be significantly influenced by interaction with the metal-support. For the graphite substrate only $Au_8$ was susceptible to being oxidized, contrasting with the silica case, where other-numbered clusters tended to show higher reactivity towards oxidation. Thus, it is admissible to expect some preferential interaction between Au atoms and Al or O atoms in alumina, depending on Au cluster size. The fact that either HBE peaks surge exclusively in the O 1s and Al 2p spectra of Au containing samples or no new Au contribution arose in the Au 4f spectrum, besides the one above described, strongly suggests that the HBE peaks cannot be related to any new Au bond. Therefore, the features appearing in HBE values in Al 2p and O 1s spectra must originate from Al–O-like bonds, although attributable to different chemical environments.

In literature, other studies can be found that make reference to such HBE contributions. Chen et al. [16], in an XPS study of oxide film growth on Mg and Al surfaces, noticed the presence of oxygen atoms in two different chemical environments, one (the LBE peak) corresponding to oxygen atoms in the oxide lattice ($O^{2-}$) of aluminum oxide (532.1 eV) or magnesium oxide (531 eV) and the other (HBE peak) corresponding to oxygen atoms near vacancy-type defects in the oxide film (with BE close to 533.5 eV for $Al_2O_3$ and to 533.2 eV for MgO). A similar occurrence was also observed by Splinter et al. [17]. In the current study, it is thus suggested that the HBE peaks probably originate from Al–O bonds related to atoms situated in sites adjacent to metal cation vacancies. The integration of Au in the oxide lattice is thermodynamically less stable than for the Al atoms and could lead to a more defective environment during film growth. Furthermore, these defects can be created by the procedure used for XPS analysis, as will be shown later.

With the gold increase in the coatings, besides the peak at $85 \pm 0.1$ eV, a new peak at lower BE ($84.1 \pm 0.1$ eV) started to occur. If for the sample with intermediate gold concentration (3.5% at. Au) it is a minor contribution it becomes the major peak in the sample with the highest gold content (7.6% at. Au). This new peak is positioned close to the BE of bulk gold, suggesting the progressive enlargement of the clusters with the increase in gold concentration. Therefore, these results seem to indicate that the samples always contain gold in different states, isolated atoms, small (metallic clusters) and very small (non-metallic) particles. Although this coexistence was observed before by, e.g., Qian et al. [18] for Au particles dispersed in $SiO_2$, the existence of Au–Au "bulk-like" bonds in the Au 4f XPS spectrum (characteristic of clusters with sizes bigger than 2–4 nm) in the as-deposited samples contradicts what was observed in XRD analysis, where no Au fcc peak could be detected. In order to shed some light on these contradictory results, a closer analysis of the XPS spectra registered before and after each progressive step of $Ar^+$ sputtering was performed.

For the sample with 7.6% at. Au, the Au 4f surface spectrum (Fig. 2(c)) obtained before ion bombardment shows: (i) a small

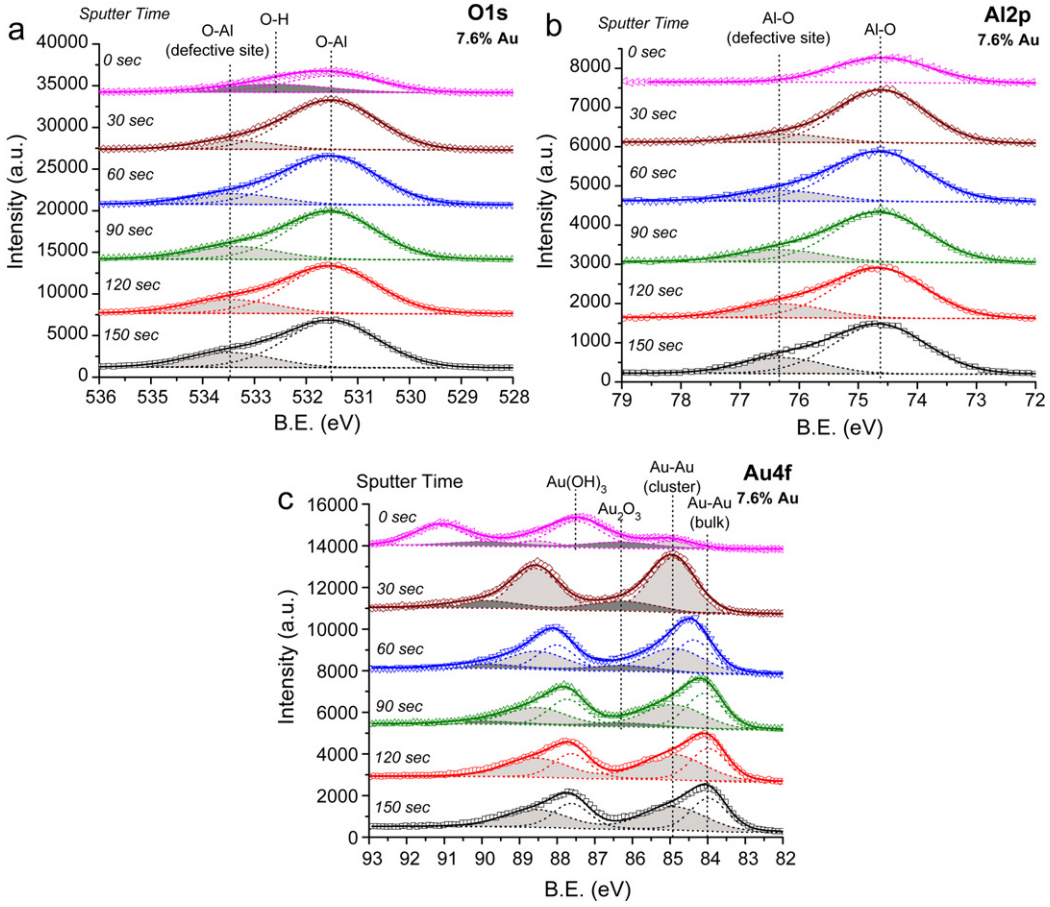


**Fig. 2.** Depth profiles of (a) O 1s; (b) Al 2p; and (c) Au 4f, XPS spectra of the AlO–Au sample with more Au content (7.6% at. Au) as a function of ion etching time.

peak located at 84.9 eV, which, as discussed above, is attributed to Au in the form of very small nanoparticles; (ii) a HBE peak, located around 87.5 eV, characteristic of Au-oxide in the hydrated form, possibly $Au(OH)_3$ in good agreement with the literature ([19] and [20]) and confirmed in the O 1s spectrum (Fig. 2(a)) by the HBE peak at 532.6 eV; (iii) a small peak at 86.3 eV, which can be tentatively attributed to a non-hydrated Au-oxide compound [19]. The second contribution, corresponding to gold(III) hydroxide, should be originated after deposition, with the contact of the sample with the moisture of the atmosphere. The latter peak is only detected for this sample with the highest Au content and it is interpreted on the basis of isolated Au atoms in substitution of Al in the amorphous alumina network. If the Au content is high enough, which is not the case for the samples with lower Au content, it is possible in some cases to simulate Au coordination; as in $Au_2O_3$. For lower Au contents, the presence of Au atoms in substitution of Al can also be envisaged but the probability that the exact coordination of $Au_2O_3$ occurs in a particular place is much lower.

After the first step of $Ar^+$ sputtering the contamination layers were removed and the hydrated peak ($Au(OH)_3$) vanished. Only the other two peaks could be observed in the Au 4f spectrum (Fig. 2(c)), the major one at 84.9 eV (very small clusters) and the small one at 86.3 eV (corresponding to the non-hydrated Au-oxide compound). With further $Ar^+$ bombardment, a new peak starts to be detected, firstly around 84.4 eV and then stabilizing close to 84 eV, the BE value characteristic of the Au–Au bulk bond. These results suggest cluster growth induced by the sputtering process. The $Ar^+$ bombardment has a double effect on the surface layers: firstly, the transfer of the kinetic energy of the ions to the surface atoms favors Au diffusion and aggregation and, secondly, breaking the low energy bond of Au–O, locally creates metal cation defect sites. Therefore, the detection by XPS after surface ion cleaning of either the Au–Au bulk bond peak in the Au 4f spectrum (Fig. 2(c)) or the HBE peaks in O 1s and Al 2p spectra (Fig. 2(a) and (b)) are now understood.

This is clearly shown in Fig. 2(a) for the evolution of the O 1s core level with sputtering time. After the removal of the first contamination layers, the hydroxide peak near 532.6 eV disappeared (in good agreement with the Au 4f profile) and the HBE peak located around 533.3 eV, attributed above to oxygen atoms near site defects, starts to be detected. This peak increased in area with sputtering time, showing the increasing removal of Au atoms (clustering) leaving more and more cation vacancy-type defect sites. Similarly, for the Al 2p XPS spectra (Fig. 2(b)) the small HBE peak located near 76.2 eV progressively increased in area with sputtering time, following the same trend as O 1s.

An alternative interpretation can be suggested for the HBE peaks in the Al 2p and O 1s spectra, by admitting the presence of localized charging in particular regions of the surface (non-uniform surface charging). With the cluster growth (after the successive sputtering steps), the "Au clusters" peak positioned in the Au 4f spectrum at ~85 eV has an additional contribution from the charging of some of the larger Au clusters (located around ~84 eV). As a consequence, the broadening of the HBE Au4f peak can be attributed to both the final state effects and the charging of some of the bigger clusters arising from non-uniform surface charging.

For the samples with lower Au contents (0.6 and 3.6 at.% Au) the spectra at the surface are very similar, with the predominance

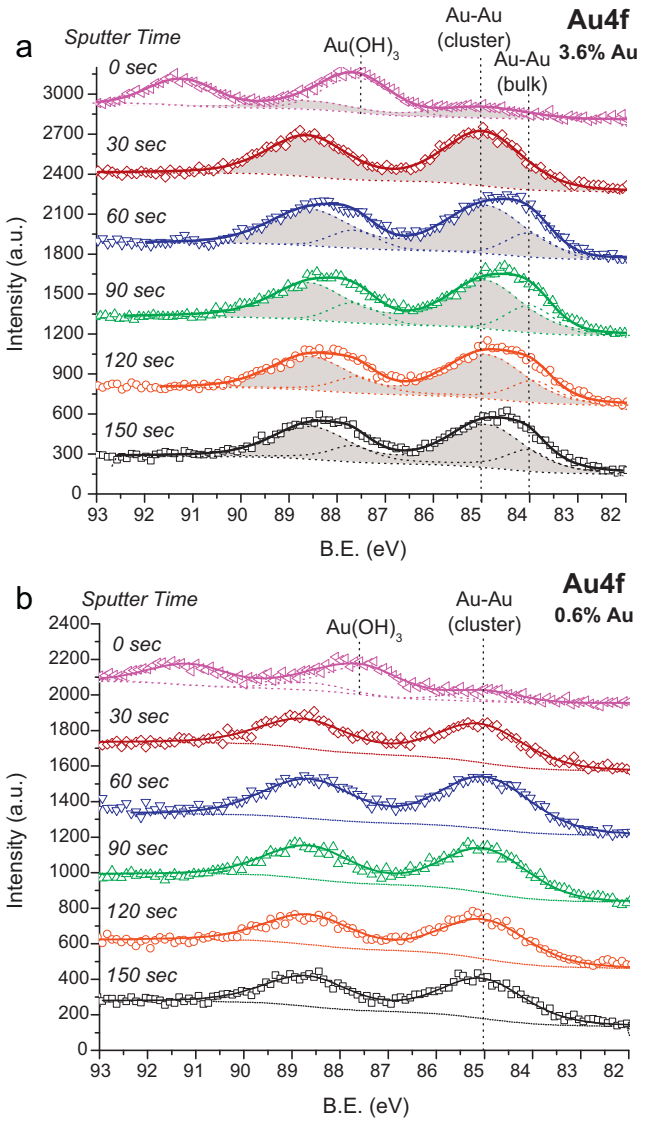


**Fig. 3.** Depth profiles of Au 4f XPS spectra of AlO–Au coatings with different Au contents, (a) 3.6 at.% Au (b) 0.6 at.%, as a function of ion etching time.

of the hydroxide peak and the small peak located close to 85 eV and corresponding to the very small Au clusters. In no case did the peaks related to the $Au_2O_3$ phase have to be considered to ensure a good fit during spectra deconvolution. After the first step of surface cleaning, both the disappearance of the hydroxide peak and an increase in the intensity of the Au-bonds in small clusters were observed for both samples. The positive shifts of approximately 1 eV in relation to Au–Au bulk gold suggest clusters with dimensions less than 0.5–1 nm (usually these dimensions correspond in the literature to the maximum shifts that are observed; see e.g., [11] and [14]). This step should represent the real structure of the coatings in the as-deposited state. For the 3.6 at.% Au sample (Fig. 3(a)), further ion bombardment made a new LBE peak appear, originating from the Au–Au bulk-like bonds, similar to what was described for the 7.6 at.% sample, meaning that cluster growth occurred during ion bombardment. The sample with the lowest Au content (Fig. 3(b)) only showed a single peak (~85 eV) even after the maximum sputtering time studied in this investigation. This must be related to the much higher spacing existing between Au atoms/aggregates in this case (due to decreased volume fraction of Au in the matrix).

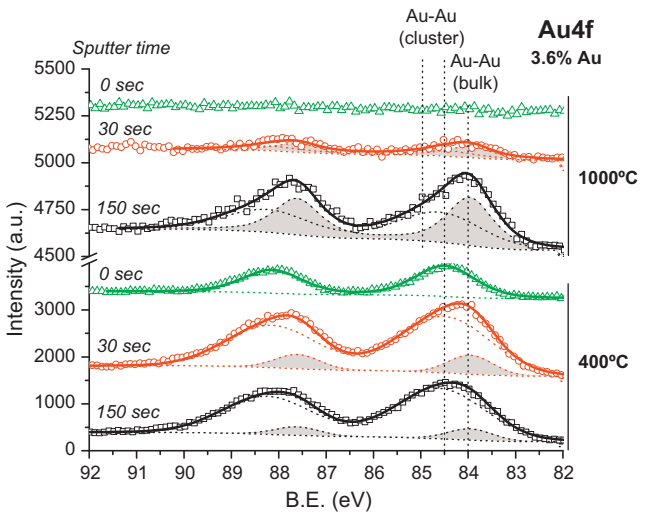


**Fig. 4.** Au 4f XPS spectra for the Al–O + Au sample with 3.6% at. Au after annealing at 400 °C and 1000 °C, as a function of ion etching time.

### 4.2. Annealed samples

In order to understand the influence of the annealing temperature on the structure of the Au-doped coatings, the sample with 3.6 at.% Au was annealed at 2 different temperatures, 400 °C and 1000 °C. For comparison, the coating without Au was also annealed at 400 °C. In the latter case, no visible changes in the XPS spectra were found regarding the position, shape and area of the peaks, when compared to the as-deposited condition, before and after the different steps of ion sputtering.

For the Au-containing coating, after annealing at 400 °C, before $Ar^+$ bombardment, a new peak in the Si 2p range with a BE of ~102.8 eV, corresponding to the Si–O bond of the $SiO_2$ compound is shown [21,22]. In agreement with this, a HBE peak at 532.7 eV was detected in the O 1s spectrum [22]. This is an expected result since the coatings started to flake off locally at this temperature due to the formation of blisters, exposing the oxidized silicon substrate. Furthermore, in contrast to the as-deposited samples, no $Au(OH)_3$ compound was detected in the Au 4f region (Fig. 4). As the temperature increases it is expected that $Au(OH)_3$ decomposes into metallic Au [19,20]. However, as the sample again comes in contact with the atmosphere, it would be expected to react again with the humid air, forming the $Au(OH)_3$ compound. The non-detection of this bond points to cluster growth, with the consequent diminishing of reactivity [23], in good agreement with the literature. Park et al. [20] got similar results while studying the oxidation of Au clusters deposited onto $Al_2O_3$; the oxidized gold species, both $Au_2O_3$ and $Au(OH)_3$,mostly decomposed into metallic species after annealing at 400 °C. This is confirmed by the only peak present in the Au 4f surface spectrum, with BE close to 84.5 eV; the shift of +0.5 eV in relation to the Au–Au bulk signal is much lower than the +1.0 eV shift verified on the as-deposited sample, indicating increased cluster size, probably from 0.5–1 nm to 1–2 nm. However, no Au peak was found in the corresponding XRD spectrum, which can be explained by the existence of gold particles with sizes below 2 nm (since the lowest threshold for a coherent domain of diffraction should be around 1–2 nm [24,25]). Furthermore, structures with low symmetry are expected for clusters with these sizes in accordance with some experimental and theoretical studies where the low energy structures of gold clusters were predicted [26,27]. The Al–O bond was confirmed in both the Al 2p and O 1s spectra by the presence of two peaks with BE at 74.6 eV and 531.6 eV, respectively. The small positive shift in the O 1s peak (+0.1 eV) of the as-grown sample could suggest a decreased tendency for

electronic transfer from the Au atoms to the oxide matrix with temperature increase, due to the progressive change from dispersed Au atoms/smaller aggregates to increasingly larger Au nanoparticles.

The Au 4f peak at 400 °C after ion etching (Fig. 4) shows an additional peak at ~84 eV which, as explained above, corresponds to the Au–Au metallic bond. Interestingly the FWHM of the 84.5 eV contribution greatly increased from 1.5 eV at the surface to ~2.1 eV in the remaining profile depth curves. The line-width observed at the surface is in accordance with what was found in theory and experiments, i.e. a progressive diminishing of the FWHM peak with the reduction of the core level BE shift. This is due to an increased relaxation originating from the rise in the number of atoms in the metal aggregates. Immediately after the start of $Ar^+$ sputtering, there should be a continuous clustering of Au atoms that are dispersed in the matrix leading to a greater size distribution. Consequently, the presence of peaks with different shifts in the XPS spectrums (from different emissions) is perceived as a single peak with increased FWHM. The clusters larger than ~4 nm will give rise to the LBE contribution detected in the Au 4f spectra at ~84 eV. Depth profiling did not change the Al 2p and O 1s spectra, with the two major peaks placed at 74.6 eV and 531.6 eV, respectively. On the O 1s, as well as on the Si 2p spectra, the peak related to the Si–O bond disappeared after the first sputter step. In the Si 2p spectrum only a peak at ~100.3 eV was afterwards observed, attributed to the Si–Si bond [6], meaning that only a minor top part of the exposed silicon was oxidized. Moreover, the HBE peaks (presented in the O 1s and Al 2p spectrums), that were observed on the as grown samples, are detected with similar positions and shapes throughout the profile of the annealed film, thus suggesting that cation metal vacancies are retained despite the temperature and the sputtering.

After annealing at 1000 °C (1 h), a depletion of Au close to the surface of the film was observed (Fig. 4). At the original surface, no trace of Au could be detected in the Au 4f spectrum. However, immediately after the first step of surface layer removal, a small Au 4f contribution could be distinguished, that progressively increased in area with the sputter time. The $4f_{7/2}$ peak was composed of two distinct contributions: (i) a major one with BE of ~84 eV, characteristic of the Au atoms in bulk gold, thus confirming the results of XRD analysis with the presence of Au nanoparticles with sizes of approximately 10 nm, a value estimated by the Scherrer equation, and (ii) a smaller one at BE close to ~84.5 eV, characteristic of Au atoms in clusters with sizes inferior to 2 nm. For this second peak, its FWHM increases progressively from 1.5 eV, after 30 s of sputter time, to 2.1 eV in the last profile curve, after 150 s of $Ar^+$ sputtering. This enlargement suggests a broadening in the range of cluster sizes with sputter time, from isolated atoms to 1–2 nm. The final structure of the coatings should thus consist of a bimodal distribution of Au, with large Au clusters (~10 nm) and the remaining Au distributed in the oxide matrix atomically or in the form of very small precipitates.

All the profile curves of the O 1s spectrum showed a contribution at BE of 532.6 eV, which neatly fits the O–Si bond of the fully oxidized silicon ($SiO_2$) of the exposed substrate zones. In good agreement with this, the Si 2p spectrum shows only one peak at ~102.8 eV (Si–O in $SiO_2$), with similar shapes in all the profile curves, indicating that the oxidation of the Si substrate underwent several nanometers in depth. Overlapping in this zone, on the O 1s spectrum, the HBE peak attributed to the vacancy defect-type sites should likely exist. The presence of an HBE peak in the Al 2p spectra corroborates this possibility.

## 5. Conclusion

On the basis of the EPMA, XRD and XPS results, the proposed structure of the film is that of a phase-separated material consisting of a mixture of an $Al_2O_3$ matrix coexisting with Au in the form of small or very small clusters (sizes < 1–2 nm). The Au element is also integrated into the oxide network with a probable $Au_2O_3$ environment, especially for the film with the highest Au content, 7.6% at. Au, where the probability that at a particular site the occurrence of the exact coordination of $Au_2O_3$ is higher. All the as-grown coatings containing Au presented at the surface a small amount of Au hydroxide. The Au oxide phases have no long-range order detectable by XRD and the Au phase is present in the form of aggregates with sizes smaller than 1 nm, thus being also out of the range of XRD detection. Cluster growth was promoted with temperature increase. After annealing at 400 °C, in the sample with intermediate amounts of Au (3.6% at.) the Au clusters were enlarged from 0.5–1 nm to 1–2 nm, but were still not detected by XRD, suggesting an amorphous structure. For annealing at 1000 °C the results indicate the coexistence in the oxide matrix of bigger clusters (with sizes close to 10 nm) together with some smaller ones (<1–2 nm) originating from Au atoms that were initially trapped in the matrix.

## Acknowledgements

This research is partially sponsored by FEDER funds through the program COMPETE-*Programa Operacional Factores de Competitividade* and by national funds through FCT-*Fundaçã o para a Ciência e a Tecnologia*, under the project DECOMAT: PTDC/CTM/70037/2006.

## References

[1] J.W. Niemantsverdriet, Spectroscopy in Catalysis—An Introduction, Wiley-VCH Verlag GmbH, Weinheim, 2000.
[2] Q. Fu, T. Wagner, Surf. Sci. Rep. 62 (2007) 431–498.
[3] D. Sarid, W.A. Challenger, Modern Introduction to Surface Plasmons—Theory Mathematica Modeling Applications, Cambridge University Press, UK, 2010.
[4] C.D. Wagner, W.M. Riggs, L.E. Davis, J.F. Moulder, G.E. Muilenberg, Handbook of X-ray Photoelectron Spectroscopy, Perkin-Elmer Corporation, Minnesota, 1978.
[5] D. Wolf, S. Yip, Materials Interfaces: Atomic-level Structure and Properties, Chapman & Hall, London, 1992.
[6] P. Sangpour, O. Akhavan, A.Z. Moshfegh, M. Roozbehi, Appl. Surf. Sci. 254 (2007) 286–290.
[7] B.L. Moroz, P.A. Pyrjaev, V.I. Zaikovskii, V.I. Bukhtiyarov, Catal. Today 144 (2009) 292–305.
[8] C. Xu, T. Sritharan, S.G. Mhaisalkar, M. Srinivasan, S. Zhang, App. Surf. Sci. 253 (2007) 6217–6221.
[9] D.C. Lim, R. Dietsche, G. Gantefor, Y.D. Kim, Size-selected Au clusters deposited on $SiO_2$/Si: stability of clusters under ambient pressure and elevated temperatures", Appl. Surf. Sci., in press, doi:10.1016/j.apsusc.2009.05.071.
[10] C.N.R. Rao, V. Vijayakrishnan, H.N. Aiyer, G.U. Kulkarni, G.N. Subbanna, J. Phys. Chem. 97 (1993) 11157–11169.
[11] M.G. Mason, Phys. Rev. B 27 (1983) 748–762.
[12] T.T. Magkoev, K. Christmann, A.M.C. Moutinho, Y. Murata, Surf. Sci. 515 (2002) 538–552.
[13] D.C. Lim, Y.D. Kim, Letter to the editor, Appl. Surf. Sci. 253 (2006) 2984–2987.
[14] D.C. Lim, I. L–Salido, R. Dietsche, M. Bubek, Y.D. Kim, Angew. Chem. Int. 45 (2006) 2413–2415.
[15] D. Dalacu, J.E. K–Sapieha, L. Martinu, Surf. Sci. 472 (2001) 33–40.
[16] C. Chen, S.J. Splinter, T. Do, N.S. McIntyre, Surf. Sci. 382 (1997) L652–L657.
[17] S.J. Splinter, N.S. McIntyre, W.N. Lennard, K. Griffiths, G. Palumbo, Surf. Sci. 292 (1993) 130–144.
[18] K. Qian, Z. Jiang, W. Huang, J. Mol. Catal. A: Chem. 264 (2007) 26–32.
[19] P.M.A. Sherwood, J. Vac. Sci. Technol. A 9 (1991) 1493–1500.
[20] E.D. Park, J.S. Lee, J. Catal. 186 (1999) 1–11.
[21] J. Koo, S. Kim, S. Jeon, H. Jeon, Y. Kim, Y. Won, J. Korean Phys. Soc. 48 (2006) 131–136.
[22] N. Bogdanchikova, A. Pestryakov, M.H. Farias, J.A. Diaz, M. Avalos, J. Navarrete, Solid State Sci. 10 (2008) 908–914.
[23] B. Hvolbaek, T.V.W. Janssens, B.S. Clausen, H. Falsig, C.H. Christensen, J.K. Norskov, Nanotoday 2 (2007) 14–18.
[24] N.M.G. Parreira, T. Polcar, A. Cavaleiro, Surf. Coat. Technol. 201 (2007) 7076–7082.
[25] J. Wang, W.M. Lau, Q. Li, J. Appl. Phys. 97 (2005) 114304.
[26] A. Sebetci, Z.B. Guvenç, Model. Simul. Mater. Sci. Eng. 13 (2005) 683–698.
[27] T.G. Schaaff, M.N. Shafigullin, J.T. Khoury, I. Vezmar, R.L. Whetten, W.G. Cullen, P.N. First, J. Phys. Chem. B 101 (1997) 7885–7891.